Solid Freeform Fabrication 2018: Proceedings of the 29th Annual International Solid Freeform Fabrication Symposium – An Additive Manufacturing Conference
Reviewed Paper

Effects of Thermal Camera Resolution on Feature Extraction in Selective Laser Melting

Xin Wang, Cody S. Lough, Douglas A. Bristow, Robert G. Landers, and Edward C. Kinzel
Department of Mechanical and Aerospace Engineering, Missouri University of Science and Technology, Rolla, MO 65409

Abstract

Selective Laser Melting (SLM) is a common additive manufacturing process which uses a laser energy source to fuse metal powder layer by layer. Engineering properties and microstructure are related to the part's thermal history. It is important to measure the thermal history in-situ to qualify parts and provide the sensing which is necessary for process control. A common measurement tool for this purpose is a thermal camera that records the thermal emission of the part's surface.

This study investigates the effects of spatial sampling resolution of thermal cameras when monitoring the temperature in SLM processes. High-fidelity simulation of an SLM process is used to quantify the effects of the camera's sampling in space. Next, the effect that spatial resolutions have on feature extraction, namely peak temperature and melt pool morphology, is investigated by applying feature extraction methodologies to the down-sampled simulation data. Finally, some methods of refining the down-sampled data are applied and their effects are discussed.

1. Introduction

Selective Laser Melting (SLM) is a common metal additive manufacturing process. The process parameters determine the microstructure and, thus, the engineering properties. Infrared (IR) imaging is a non-contact detection method which is feasible for the in-situ monitoring of SLM processes [1]. The authors concluded that the thermal camera was able to capture the melt pool dimensions. However, the errors caused by quantization (digitization) in the binarized image was not considered (Fig. 1 (c)). They also related the lengths and widths of the melt pools with the laser scanning speeds, while these metrics are only measured from the binarized images [2]. Regarding the low-resolution temperature profile, they interpolated points into it. Wegner and Witt [3] used a thermal camera in the laser sintering process. They used the melt's temperature as an indicator of process parameters and related it with laser exposure time and laser power. An IR camera was shown to be also effective in locating defects during the SLM process of 6H-SiC [4].

Work performed and funded by The Department of Energy's Kansas City National Security Campus is operated and managed by Honeywell Federal Manufacturing & Technologies, LLC under contract number DE-NA0002839.

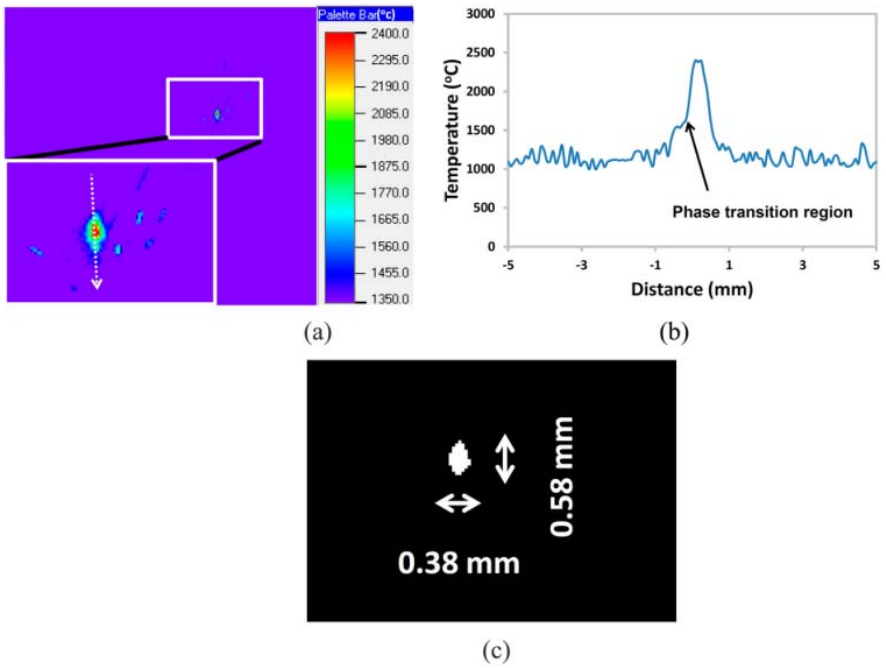

Fig. 1: Example of melt pool monitoring in an SLM process using a thermal camera: (a) thermal contour, (b) radiant temperature profile along scanning direction and (c) melt pool. [1]

There are two types of thermal cameras: scanning devices and infrared Focal Plane Arrays (FPAs). The FLIR thermal camera in the experimental platform at Missouri S&T is of the latter type and has a 640×512 pixel focal plane array with a 50 megapixel clock rate allowing full frame sampling at 126 frames/sec with a 14 bit dynamic range. The photodetectors in the FLIR thermal camera are the InGaAs array, which operate in the 0.9-1.7 μm wavelength region [5].

The spatial resolution is an important parameter of the thermal camera. Each PhotoSensitive Element (PSE) in the array corresponds to one image pixel, The PSE signal can be expressed in volts, ADC units, the number of accumulated electrons, or the amount of stored charges. Its sources are always a photo current and a PSE dark current accumulated in the corresponding multiplexer capacitor [6]. In practice, the optical system can be configured to obtain a field of view at a distance from the build plate. By configuring the optical system, a higher resolution can be achieved at the expense of the range of the field of view. When observing a large part or several parts together, the resolutions of the thermal images are usually very low. A trade-off must be made between the resolution and the viewing area size. Very-Low-Resolution (VLR) problems exist in image recognition, such as very-low-resolution human face recognition [7,8].

A thermal camera has a specific resolution for a viewing area and the digital pictures are spatially discrete. The digital data can be treated as discrete samples of the continuously varying surface temperature distribution and each pixel in the picture is a single temperature measurement at its corresponding area. However, some of the spatial information will be lost by this down-sampling. In addition, the camera sensors collect the radiance inside the regions of the pixels, instead of at specific points. However, researchers often treat thermal images as discrete samples at specific grid points of surface temperature distribution and measure the melt pool's

length and width directly from the image. The errors caused by low resolution sampling are not considered sometimes.

In order to understand the effect of sampling, high-fidelity simulation results are utilized for investigation [9]. A sampling model is proposed and applied to the simulation data, and then artificial thermal images are generated. Features are measured from down-sampled images and original images separately, and their differences are just the errors caused by sampling. In other words, the measurements of the features are not exactly the real values. The down-sampling has two main effects on the feature extraction: darkening effect of the melting pools and digitization of the morphological features. The darkening effect is caused by averaging the pixels and, thus, the maximal pixel value is always smaller than the true maximal surface temperature value.

So some questions are brought up: how to understand and correct the measurements and recover the real features? In Section 2, a sampling model is proposed for the purpose of obtaining artificial low-resolution images from the original data, just like how the thermal camera works. In Section 3, the errors of the measurements of the features are plotted in figures, which shows the accuracy corresponding to the sampling grid size. In the following sections, interpolation and fitting methods are applied to the down-sampled data to find whether the methods improve the measurements.

2. Sampling Model and Temperature Measurement Model

Since it is difficult to know the real surface temperature during the process, high-fidelity simulation data [9] of surface temperature are utilized instead of the real experimental surface temperature. The simulation data should be down-sampled to generate artificial thermal images with low resolutions. Therefore a sampling model is needed.

The thermal camera collects the radiance inside the pixels over a period of time. Assuming the emissivity ε of the material is constant, the sampled radiance is given by

$$R(x_i, y_i, t_i) = k\int_{t_i}^{t_i+\Delta t}\int_{x_i-\frac{\Delta x}{2}}^{x_i+\frac{\Delta x}{2}}\int_{y_i-\frac{\Delta y}{2}}^{y_i+\frac{\Delta y}{2}} \varepsilon T^4(x, y, t)\,dx\,dy\,dt\,, \tag{1}$$

where T is the temperature inside the pixel $\left[x_i-\frac{\Delta x}{2}, x_i+\frac{\Delta x}{2}\right]\times\left[y_i-\frac{\Delta y}{2}, y_i+\frac{\Delta y}{2}\right]$ during the time $[t_i, t_i+\Delta t]$, k is the gain and R is the radiance collected by the thermal camera sensor.

Assuming that the temperature field T is constant over the pixel area, (1) becomes

$$R = kT^4(x, y, t)\Delta x\Delta y\Delta t\,. \tag{2}$$

Solving for the measured temperature in equation (2) yields

$$T_M = \left(\frac{R}{k\Delta x\Delta y\Delta t}\right)^{1/4}, \tag{3}$$

where T_M (K) is the temperature measurement. To recover the temperature from the measured radiance, one must determine the model parameters k and ε. Combining (1) and (3), the measurement function is

$$T_M = \left(\frac{1}{\Delta x \Delta y \Delta t} \int_{t_i}^{t_i+\Delta t} \int_{x_i-\frac{\Delta x}{2}}^{x_i+\frac{\Delta x}{2}} \int_{y_i-\frac{\Delta y}{2}}^{y_i+\frac{\Delta y}{2}} T^4(x, y, t) dx dy dt \right)^{1/4}. \quad (4)$$

3. Errors from Spatial Down-Sampling

The features of a melt pool, namely the peak value p and melt pool length L, width W and area A, are measured from the thermal camera in practice, and the measurements of them have errors caused by low-resolution sampling. To determine the magnitude and nature of low-resolution sampling on these critical features, this section utilizes high-fidelity simulation data and the sampling model (4).

3.1. Utilization of Simulation Data

Simulation data of the surface temperature in the SLM process are utilized to characterize the errors resulting from the camera's spatial resolution. Using the down-sampling model, low-resolution images are obtained from the simulation data, which are used to investigate the errors caused by down-sampling. A piece of simulation video data is utilized for the investigation of sampling. In the simulation, the element size is $\Delta x = \Delta y = 10$ μm and time step is $\Delta t = 1$ μs. The laser power is set to be 200 W and the laser pulse period is 90 μs. During each laser pulse period, the exposure time is 75 μs, and the laser is off for the 15 μs. The laser point distance is 60 μm. These manufacturing process parameters are often used when fabricating parts with 304L stainless steel [10]. The top and side views of a simulation frame are given in Fig. 2 and Fig. 3 respectively.

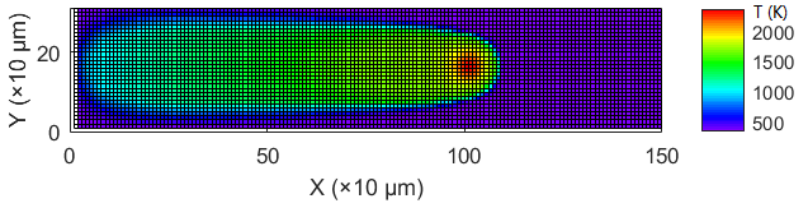

Fig. 2: One Frame of Simulation

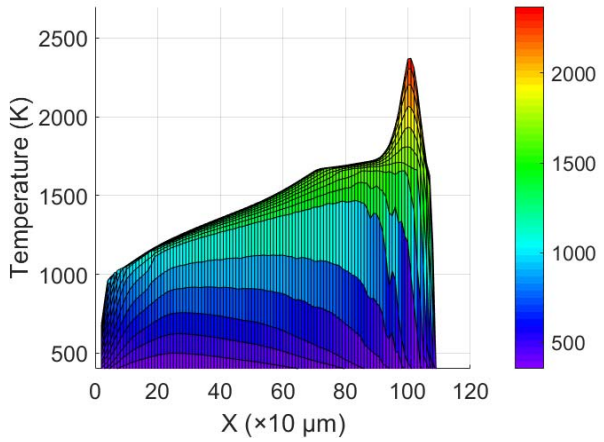

Fig. 3: Surface Temperature of a Simulation Frame (Lateral View)

In this discrete case, where only spatial sampling is considered, equation (4) can be written as

$$T_M(i, j, s_1, s_2, r) = \left(\frac{1}{r^2} \sum_{m=r(j-1)+1}^{rj} \sum_{n=r(i-1)+1}^{ri} T^4(m+s_2, n+s_1) \right)^{1/4}, \quad (5)$$

where $T(m, n)$ denotes the value at (m, n) in the original frame and $T_M(i, j, s_1, s_2, r)$ denotes the value at (i, j) in the down-sampled frame with camera grid shifting (s_1, s_2), and r is the down-sampling rate. In addition to the lower sampling rate r, it is important to note that the location of the sampling grid over the melt pool can have a critical impact on the measurements and measurement interpretation. For example, a single pixel capturing the laser spot will show a significantly higher temperature than, for instance, if the laser spot fell at the intersection of four pixels. The parameters (s_1, s_2) are used here to capture melt pool locating effects within the camera pixels. To illustrate this effect with our simulation data (already sampled), in Fig. 4 the black lattice is the original image. In this case, the down-sampling rate is $r = 5$. The shifting of the blue lattice is $(s_1 = 1, s_2 = 2)$ and that of the red lattice is $(s_1 = 2, s_2 = 3)$. While it may be possible to carefully align the camera or reconstruct the precise laser path in order to determine the precise location of the laser spot at sub-pixel accuracy, here we assume that is not possible. Therefore, we consider such the location an uncertainty and evaluate the results of our low-resolution sampling with respect to this uncertainty.

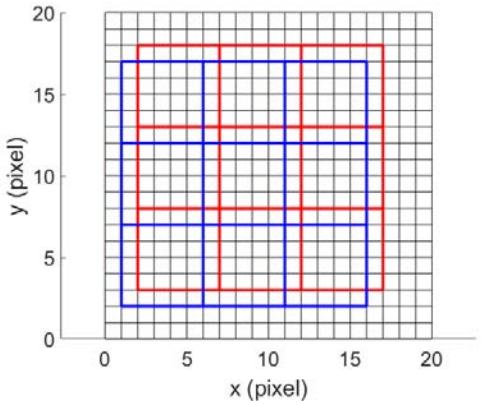

Fig. 4: Illustration of Sampling Grid Shifting

3.2. Direct Measuring Method

Direct measurements are obtained by directly extracting the features from the thermal images without data processing. Each frame is a matrix of temperatures $T(m,n)$ and the down-sampled matrix of temperatures is $T_M(i,j,s_1,s_2,r)$. The true peak temperature from the simulation is

$$p = \max_{m,n} T(m,n), \tag{6}$$

and the peak temperature in the low-resolution image is

$$p_M(s_1,s_2,r) = \max_{i,j} T_M(i,j,s_1,s_2,r), \tag{7}$$

The error caused by down-sampling with camera shift (s_1, s_2) and sampling rate r is

$$e(s,t,r) = p_M(s,t,r) - p\,. \tag{8}$$

Measurement of the length, width and area of the melt pool are typically achieved by first defining a melt thresholds. A threshold is set, the matrix is searched, and all of the pixels greater than the threshold are identified. The region above the threshold is the set

$$E = \{(x_i,y_i): T(x_i,y_i) \geq threshold\}. \tag{9}$$

The length of the melt pool is

$$L = \max\{x_i\} - \min\{x_i\}. \tag{10}$$

Similarly, the width of the melt pool is

$$W = \max\{y_i\} - \min\{y_i\}. \tag{11}$$

Suppose N is the number of points in the set E and A_p is the size of each pixel, then the melt pool area is

$$A = NA_p\,. \tag{12}$$

In the down-sampled images, the measurements are defined as above and the measured length, width, and area, respectively, are denoted by L_M, W_M and A_M. Then the length, width, area errors, respectively, are

$$e_L = L_M - L\,, \tag{13}$$

$$e_W = W_M - W\,, \tag{14}$$

$$e_A = A_M - A\,. \tag{15}$$

3.3. Errors from Down-Sampling

Down-sampling leads to two notable effects on the measurements: the darkening effect on the peak temperature (Fig. 5) and the digitization of the morphological features (Fig. 6). The first effect is that the peak temperature in the low-resolution image is always lower than the original

peak temperature. The latter effect is that only several numbers can be taken as the measurements of the melt pool's length, width and area from the low-resolution image.

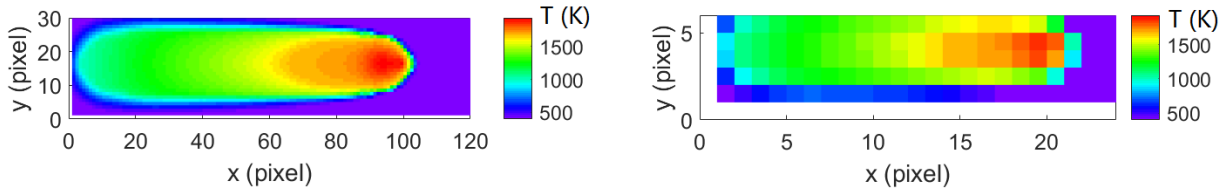

(a) Original Peak Temperature = 1924 K (b) Down-sampled Peak Temperature=1864 K

Fig. 5: Illustration of the Darkening Effect on the Peak Temperature

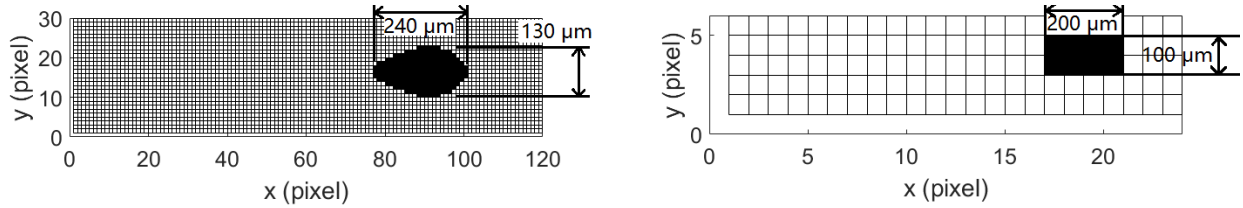

(a) Original Melt Pool (b) Down-sampled Melt Pool

Fig. 6: Illustration of the Digitization of the Morphological Features

To analyze the errors due to down-sampling, the data during one laser period are analyzed. In one experimental platform at Missouri S&T, a Renishaw system is fitted with a FLIR camera directed toward a portion of the powder bed with a 140 μm camera pixel size. We will use this value as a nominal value for analysis and therefore set the down-sampling rate at $r = 14$. In the discrete simulation data, there are $r^2 = 196$ total possible shifts in all. In this way, the distribution of the errors of the feature measurements are plotted in Fig. 7-Fig. 10. When defining the melt pool, take the threshold = 1700 K , which is the melt temperature of the material.

In Fig. 7, it is shown that the measurements of the peak temperature will always be lower than the real value and the range of the peak temperature measurements is continuous and bounded. However, as for the morphological features (length, width, area), the measurements are highly digitized (Fig. 8-Fig. 10). In Fig. 8 and Fig. 9, the measurements of lengths and widths are in discontinuous groups. The distance between the discontinuous bars is just the size the sampling grid, which is 140 μm in this case. In other words, the measurements can only be from $\{0, \Delta x, 2\Delta x, 3\Delta x, ...\}$ if the camera pixel size is Δx. The digitization phenomenon happens on the area measurements similarly, where the distance between the bars in Fig. 10 is Δx^2.

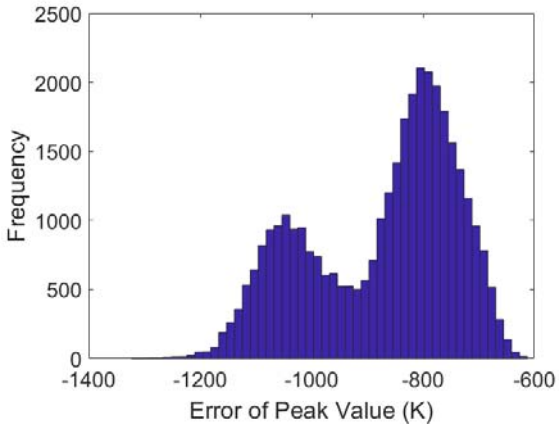

Fig. 7: Distribution of Peak Temperature Errors

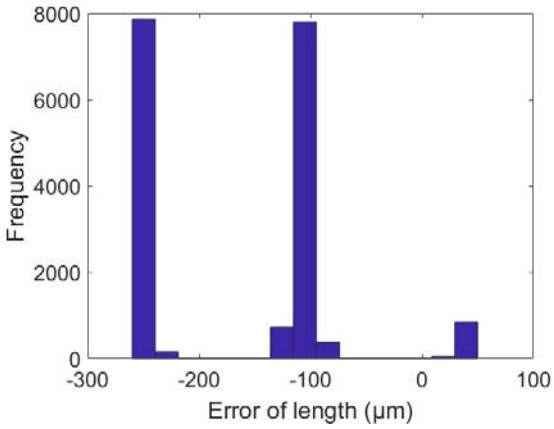

Fig. 8: Distribution of Length Errors

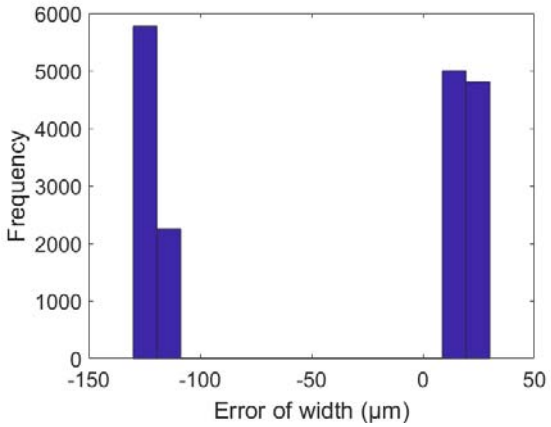

Fig. 9: Distribution of Width Errors

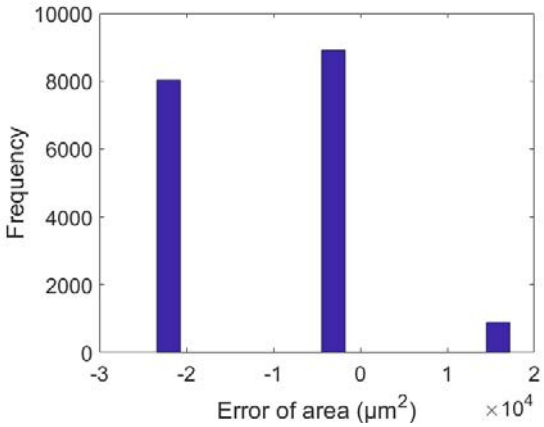

Fig. 10: Distribution of Area Errors

The effect of spatial down-sampling may be instructive for the users who monitor the SLM process by a thermal camera. When choosing a size of the sampling grid and making all possible shifts, it is meaningful to calculate the maximum, the minimum and the mean of the errors caused by sampling with all shifts. The maximum, minimum and mean errors for the peak temperature and morphological features are plotted with respect to sampling grid sizes (Fig. 11-Fig. 14). These graphs show what resolution is need in order to achieve a desired level of accuracy. At a given sampling grid size (camera resolution), the maximum and the minimum of the measurements represent the uncertainty caused by the motion of the melt pool across the camera view, when one is conducting such an experiment.

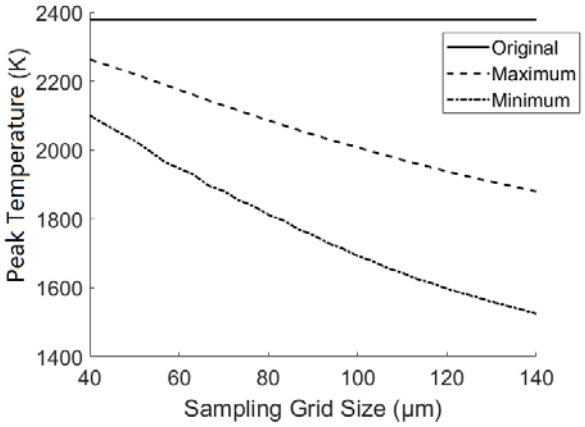

Fig. 11: Peak Temperature Errors for Different Sampling Grids

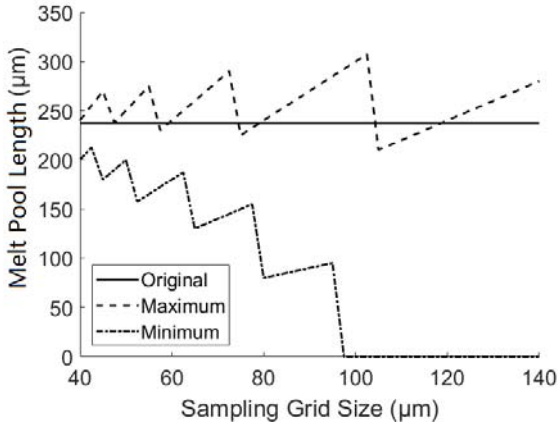

Fig. 12: Melt Pool Length Errors for Different Sampling Grids

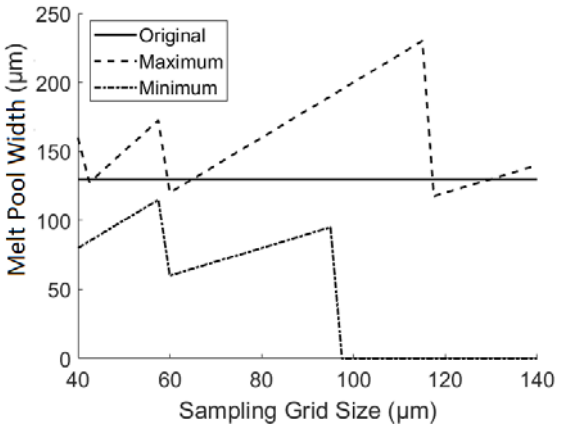

Fig. 13: Melt Pool Width Errors for Different Sampling Grids

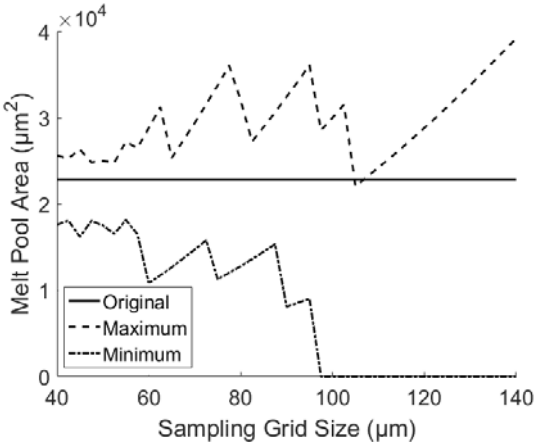

Fig. 14: Melt Pool Area Errors for Different Sampling Grids

The results from the down-sampled simulation data show that the curves of peak temperature measurements with respect to the sampling grid sizes are smoother than the morphological features. Besides, when the spatial resolution is too low, the melting region cannot be extracted after down-sampling.

4. Interpolation of Down-Sampled Images

Interpolation is commonly used in image processing of low-resolution images. In this work, linear interpolation and spline interpolation are tried. The two interpolation methods have different natures. Linear interpolation is a simple method to create more pixels in a low-resolution image, but this method cannot produce a smooth curve. They are illustrated in Fig. 15 and Fig. 16. Spline interpolation is a fitting method which uses a piecewise 3rd-degree polynomial function.

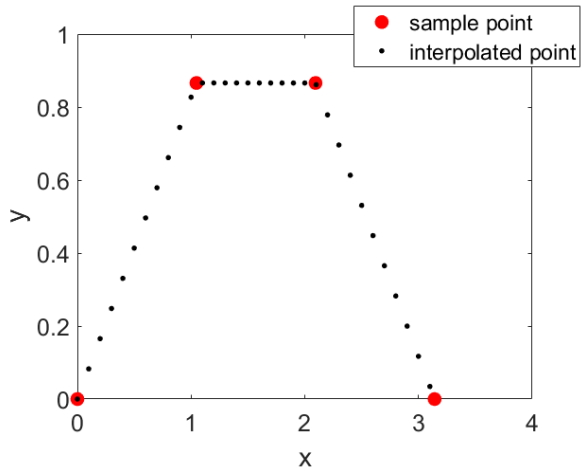

Fig. 15: Linear Interpolation

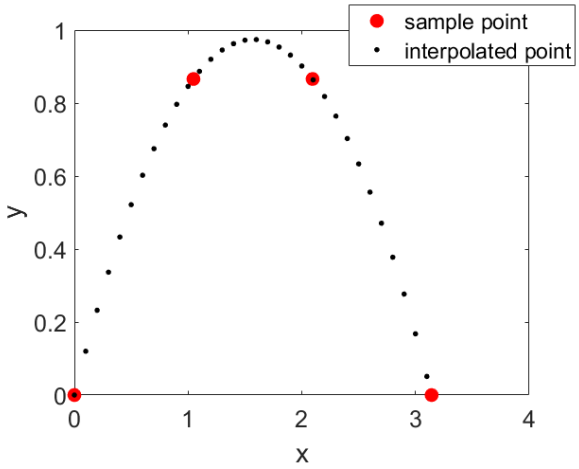

Fig. 16: Spline Interpolation

Here the 2-dimensional interpolations are applied to the artificial down-sampled images, and the interpolation rate should be such as to restore the original resolution. The following are the results of measurements after linear interpolation (Fig. 17-Fig. 20).

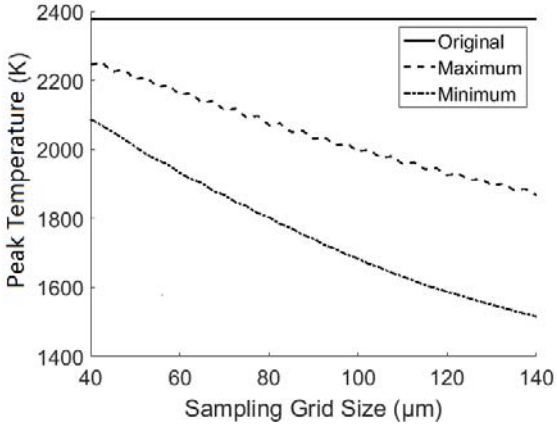

Fig. 17: Peak Temperature Errors after Linear Interpolation

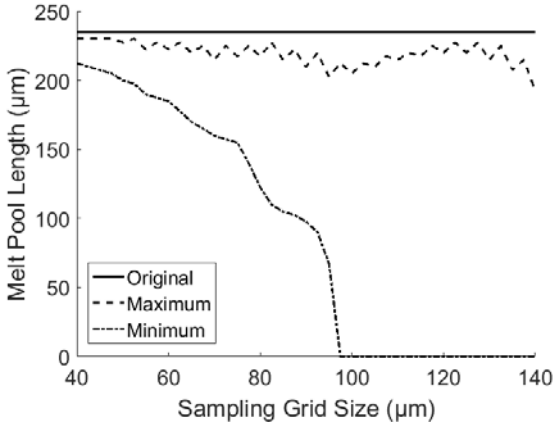

Fig. 18: Melt Pool Length Errors after Linear Interpolation

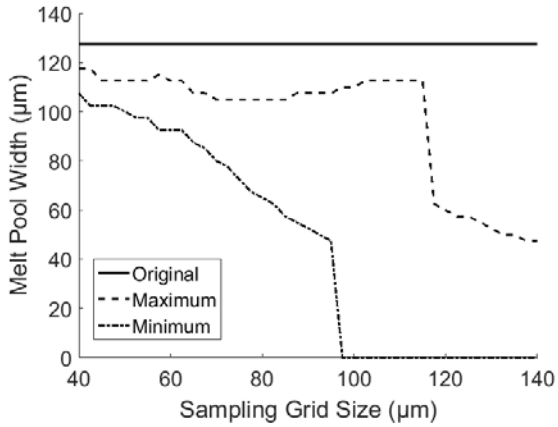

Fig. 19: Melt Pool Width Errors after Linear Interpolation

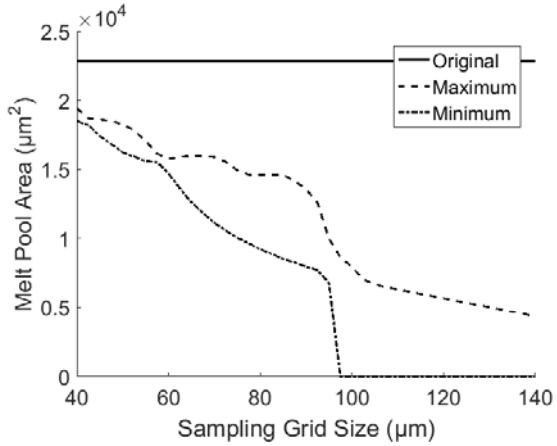

Fig. 20: Melt Pool Area Errors after Linear Interpolation

The following are the results of measurements after spline interpolation.

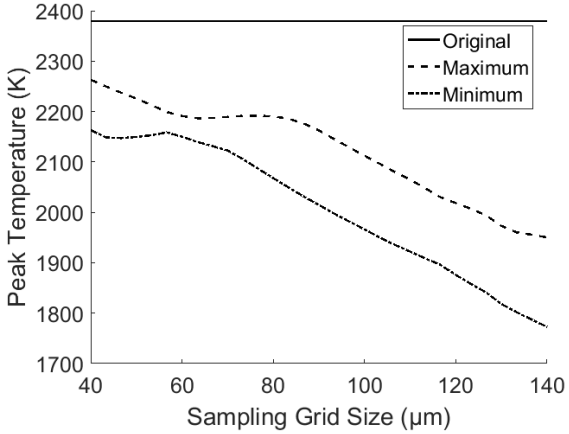

Fig. 21:Peak Temperature Errors after Spline Interpolation

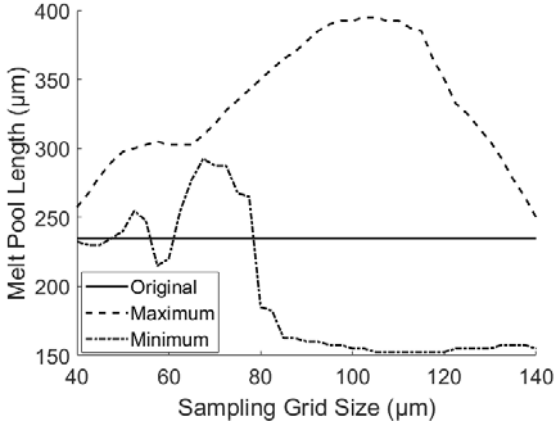

Fig. 22: Melt Pool Length Errors after Spline Interpolation

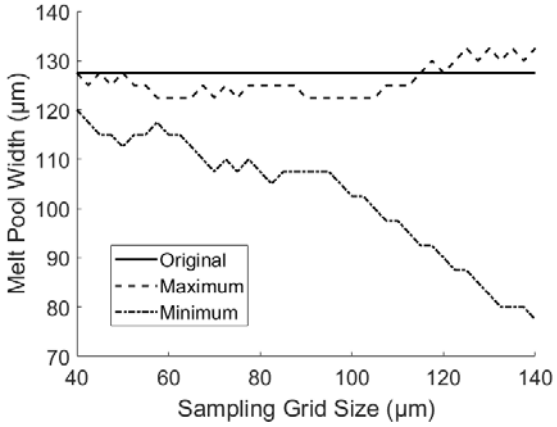

Fig. 23: Melt Pool Width Errors after Spline Interpolation

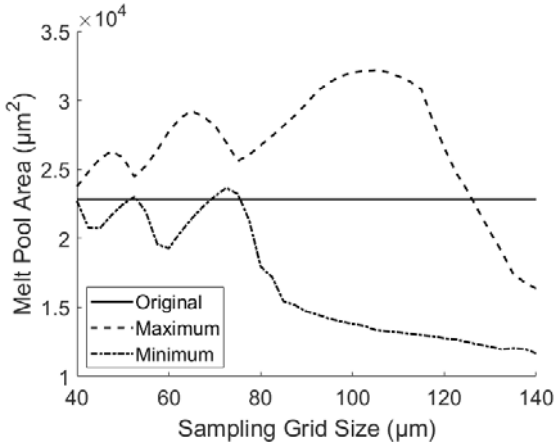

Fig. 24: Melt Pool Area Errors after Spline Interpolation

The simple linear interpolation can reduce the digitization effect a little. But linear interpolation cannot restore the peak value which is lost by sampling, just as illustrated in Fig. 15. The spline interpolation is hopeful to restore the peak value of a curve (Fig. 16). However, it does not make obvious improvements in the measurements of features, but makes the measurements worse sometimes. The reason is that interpolation methods treat every pixel point as a pointwise measurement on the original surface, but in fact the pixel value is a sort of average over the pixel region. So pointwise interpolations are not proper in the problem.

5. Fitting Method

An alternative to direct measurement from thermal camera data is to fit the measurements to a model or set of basis functions. Here, we explore a fitting method that segments the melt pool into two parts: the front part and the rear part, as illustrated in Fig. 25. The temperature of the front part is simpler and can be approximated by a Gaussian-like function

$$T(x, y) = A\exp\left(-\frac{(x-x_0)^2}{S_1^2} - \frac{(y-y_0)^2}{S_2^2}\right) + T_{amb},\ x \ge x_0\,, \tag{16}$$

where $T(x, y)$ is the surface temperature, (x_0, y_0) is the peak temperature location and T_{amb} = 353 K is the ambient temperature in the simulation. For simplicity, let $(x_0, y_0) = (0, 0)$ by coordinate system translation, and then (16) can be written as

$$T(x, y) = A\exp\left(-\frac{x^2}{S_1^2} - \frac{y^2}{S_2^2}\right) + T_{amb},\ x \ge 0\,, \tag{17}$$

The down-sampled image is shown in Fig. 26, where the sampling grid size $\Delta x = \Delta y$ =40 μm. The peak temperature after down-sampling (p_M = 2233 K) is lower than the original peak temperature (p = 2371 K).

A fitting method is proposed to have a better estimation of the peak temperature based on the low-resolution image. The penalty function is

$$P(A, S_1, S_2, x_0, y_0) = \sum_i \left(\left(\iint_{\Omega_i} T^4(s, t, A, S_1, S_2, x_0, y_0) dtds \right)^{1/4} - T_i \right)^2, \tag{18}$$

where $\Omega_i = [x_i - \Delta x/2, x_i + \Delta x/2] \times [y_i - \Delta y/2, y_i + \Delta y/2]$ and (x_i, y_i, T_i) are the data set for fitting. The optimization is fulfilled by "fmincon" function in Matlab. The estimated peak temperature from the fitting result is p_{est} = 2338 K. In this way, the estimated peak temperature is better than that from the low-resolution image.

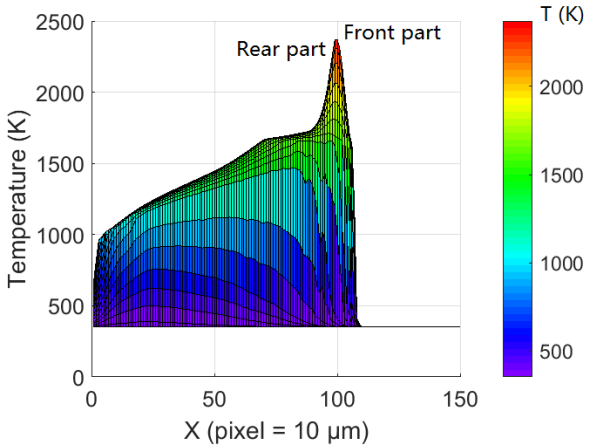

Fig. 25: Surface Temperature in Simulation

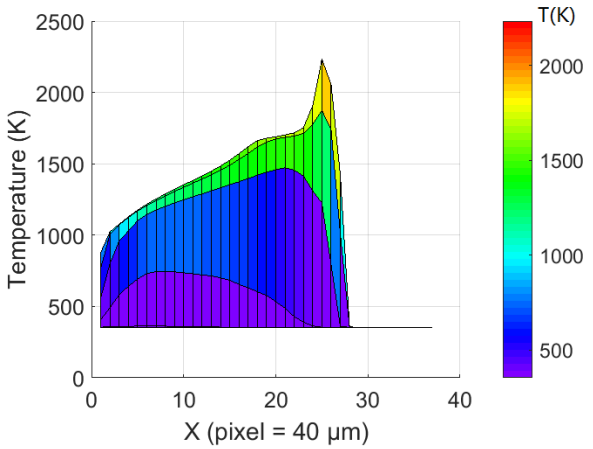

Fig. 26: Down-Sampled Surface Temperature

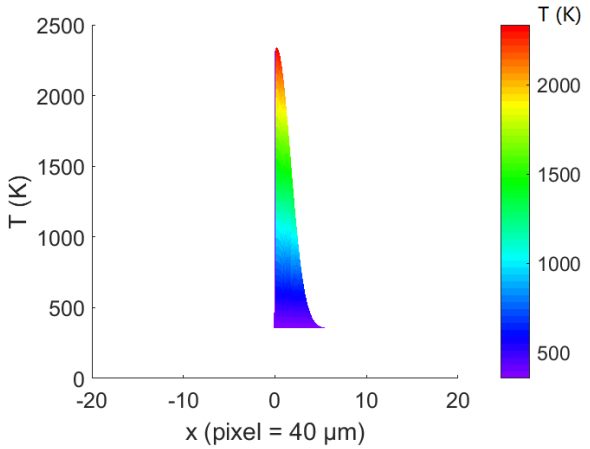

Fig. 27: Fitting Result of the Front Part of the Melt Pool

Using this method, the width of the melt pool can also be estimated. The original melt pool width is $W = 120$ μm. The down-sampled melt pool width is $W_M = 80$ μm. The estimated width is $W_{est} = 112$ μm. The fitting method can also obtain a better measurement of the melt pool width. The fitting method is based on the assumed surface temperature function. The Gaussian-like function (17) is not applicable to the rear part of the melt pool, and the existence of the phase transition region is still a challenge for the fitting method.

6. Conclusions

The thermal camera is an instrument for monitoring the SLM process. Temperature information and morphological information of melt pools are often related to manufacturing parameters and engineering properties. It is worth noting that the features extracted from low-resolution thermal images contain errors caused by spatial sampling. In this work, high-fidelity simulation data are utilized and a sampling model is proposed. Based on these, the errors caused by sampling grid sizes are plotted for all possible grid shifts. This gives the level of accuracy for a given camera pixel size, which is worth of concern in experiments. Interpolation is often used in the processing of low-resolution images, but interpolation is not enough to eliminate the effect of sampling. The model-based function fitting method can improve the measurements of the melt width and peak temperature.

7. Acknowledgement

This work was funded by Honeywell Federal Manufacturing & Technologies under Contract No. DE-NA0002839 with the U.S. Department of Energy. The United States Government retains and the publisher, by accepting the article for publication, acknowledges that the United States Government retains a nonexclusive, paid up, irrevocable, world-wide license to publish or reproduce the published form of this manuscript, or allow others to do so, for the United States Government purposes.

8. References

[1] Cheng, B., Lydon, J., Cooper, K., Cole, V., Northrop, P., & Chou, K. (2018). Infrared thermal imaging for melt pool analysis in SLM: a feasibility investigation. Virtual and Physical Prototyping, 13(1), 8-13.
[2] Cheng, B., Lydon, J., Cooper, K., Cole, V., Northrop, P., & Chou, K. (2018). Melt pool sensing and size analysis in laser powder-bed metal additive manufacturing. Journal of Manufacturing Processes, 32(November 2017), 744-753.
[3] Wegner, A., & Witt, G. (2011). Process monitoring in laser sintering using thermal imaging. 22nd Annual International Solid Freeform Fabrication Symposium - An Additive Manufacturing Conference, SFF 2011, 405-414.
[4] Lee, K. Y., Miyazaki, H., Okamoto, Y., & Morimoto, J. (2010). Characterization of Defects in Semi-Insulating 6H-SiC Substrates Using IR Thermal Imaging Camera. Materials Science Forum, 645-648, 559-562.
[5] Rogalski, A. (2012). Progress in focal plane array technologies. Progress in Quantum Electronics, 36(2-3), 342-473.
[6] Patrashin, A. I., Burlakov, I. D., Korneeva, M. D., & Shabarov, V. V. (2016). Analytical model used to calculate focal-plane-array parameters. Journal of Communications Technology and Electronics, 61(3), 311-318.
[7] Wang, Z., Miao, Z., Jonathan Wu, Q. M., Wan, Y., & Tang, Z. (2014). Low-resolution face recognition: A review. Visual Computer, 30(4), 359-386.
[8] Mostafa, E., Hammoud, R., Ali, A., & Farag, A. (2013). Face recognition in low resolution thermal images. Computer Vision and Image Understanding, 117(12), 1689-1694.
[9] Li, L., Lough, C., Replogle, A., Bristow, D., Landers, R., & Kinzel, E. (2017). Thermal Modeling of 304L Stainless Steel Selective Laser Melting. Solid Freeform Fabrication, Vol. 6061, pp. 1068-1081.
[10] Amine, T., Kriewall, C. S., & Newkirk, J. W. (2018). Long-Term Effects of Temperature Exposure on SLM 304L Stainless Steel. Jom, 70(3), 384 – 389.